



Improving field emission properties of vertically aligned carbon nanotube arrays through a structure modification

Arun Thapa¹ , Katherine L. Jungjohann² , Xuewen Wang¹ , and Wenzhi Li^{1,*}

¹Department of Physics, Florida International University, 11200 SW 8th Street, Miami, FL 33199, USA

²Center for Integrated Nanotechnologies, Sandia National Laboratories, Albuquerque, NM 87185, USA

Received: 4 August 2019

Accepted: 23 October 2019

Published online:

7 November 2019

© Springer Science+Business Media, LLC, part of Springer Nature 2019

ABSTRACT

Vertically aligned carbon nanotube (VACNT) emitters were synthesized directly on stainless steel substrate using DC plasma-enhanced chemical vapor deposition. Remarkable field emission (FE) properties, such as low turn-on electric field ($E_{TO} = 1.40 \text{ V}/\mu\text{m}$) and low threshold electric field ($E_{TH} = 2.31 \text{ V}/\mu\text{m}$), were observed from VACNT arrays with long length and moderate density. The FE performance was significantly enhanced by a uniquely bundled structure of VACNTs formed through a simple water treatment process. The FE properties of VACNTs were further improved by coating the exterior of CNTs with a uniform layer of crystalline SnO_2 nanoparticles; the E_{TO} and E_{TH} were reduced to 1.18 and 2.01 $\text{V}/\mu\text{m}$, respectively. The enhancement of FE properties by SnO_2 coating can be attributed to the morphological change of VACNTs caused by the solution phase coating process. The coated samples also exhibited an improved FE stability which is attributed to the enhancement of the mechanical strength and chemical stability of the VACNTs after the SnO_2 coating. The VACNT emitters with characteristic features such as a conductive substrate, low contact resistance between the VACNTs and the substrate, uniform coating, and bundled morphology can be ideal candidates for FE devices.

Introduction

Materials designed and developed with advanced concepts can help the development of new devices and improve many components of current technologies. A power-efficient, high-current, and low-temperature electron emitter, unlike thermionic emitter,

is essential for many simple to complex advanced vacuum electronic devices. Carbon nanotubes (CNTs), known for their superior mechanical [1], thermal [2], electrical [3] properties as well as high aspect ratio [4], are regarded as the best field emitters in a non-oxidizing environment. CNT array can be utilized as cold field emitters in vacuum electronic

Address correspondence to E-mail: Wenzhi.Li@fiu.edu

devices such as FE displays [5], electron microscope [6], X-ray sources [7], microwave amplifiers [8], and nano-electronics [9]. Apart from being more energy-efficient, CNT field emitters can produce more stable electron beam which can be helpful for an accurate electron beam focusing.

Generally, CNTs are synthesized on a metallic substrate which is coated first with a buffer layer and then a catalyst layer by different deposition techniques. The buffer layer arguably adds an extra electrical resistance between the CNT and the metal substrate, and hence, it can compromise the FE performance of the CNT field emitters. Low ohmic contact between the metallic substrate and the CNTs is one of the crucial factors to lower the turn-on electric field as a result of easy electron transport from the substrate to the CNTs, and hence to the vacuum [10]. Further, the ohmically contacted CNT emitters can withstand a high emission current during the FE process. It is believed that the CNT's tip releases the electrons during the FE process. So, vertically aligned carbon nanotubes (VACNTs) have been grown to facilitate the FE process so that the tip of each VACNT experiences the same electric field to emit the electrons. The need for growing VACNTs directly on a conducting substrate and the effect of other factors such as density and structural changes of VACNTs on FE properties have been addressed in many reports. Talapatra et al. [11] reported a direct synthesis of aligned CNTs on an Inconel substrate by chemical vapor deposition (CVD) method and discussed the necessity of growing CNTs on a bulk conducting substrate for applications in FE devices. Neupane et al. [12] synthesized VACNTs arrays directly on stainless steel (SS) substrates by plasma-enhanced chemical vapor deposition (PECVD) method and observed a better FE performance (low turn-on electric field, low threshold electric field, and high field enhancement factor) compared to that from VACNTs grown on a catalyst-coated stainless steel substrate. Bonard et al. [13] also reported a superior FE performance of medium density VACNTs in comparison with that of high and low density VACNTs grown on a silicon substrate by the CVD method. Kim et al. [14] highlighted the importance of growing VACNTs with an optimum normalized spacing (s/l , where s is the spacing between CNTs and l is the CNT length) so that electrostatic interaction among the CNTs can be minimized to attain better FE performance. There are several reports on

improving the FE performance of VACNTs by improvised synthesis through substrate modification, such as VACNT-based pillar structure [15–18]. It is reported that the coating on the CNT wall by nanoparticles, such as TiO_2 , ZnO , RuO_2 , MgO , In , Al , and Cu , not only modify the electronic structure of the CNT but also helps to passivate defective sites on the CNT surface [19–25]. This can lead to highly conductive, mechanically, and chemically more stable CNTs composite, resulting in an enhanced FE performance. To our knowledge, only a few works regarding the direct synthesis of VACNT-based field emitters on the conducting substrate and their FE properties enhancement by simple posttreatment methods such as water treatment and SnO_2 coating have been reported. The main focus of this study was to grow VACNT arrays directly on the SS substrate without the addition of buffer and catalyst layers and to enhance the FE properties of the VACNT-based field emitters by the water treatment and SnO_2 coating to the pristine VACNT arrays.

In this paper, we report a direct growth of VACNTs on SS substrate without buffer and catalyst layers on top of the substrate surface by a PECVD method. We further successfully coated the VACNTs with a uniform layer of SnO_2 nanoparticles using a facile one-step wet-chemical method. The FE characteristics of the as-synthesized, water-treated, and SnO_2 -coated VACNTs were studied to understand the effect of the SnO_2 coating as well as the morphology change of VACNTs array on the FE performance. Our results show that water treatment and SnO_2 coating can lead to significant improvement in the FE properties of the VACNTs. We also performed simulations to understand the effect of bundling of the CNTs on the FE performance of the VACNTs emitters. The simulation result agrees well with experimental results.

Experimental details

VACNT arrays were grown on SS 304 type by PECVD method as described in detail in our previous work [26]. In brief, as shown in the schematic in Fig. 1, a small piece of SS sheet, of an area about $1 \times 1 \text{ cm}^2$ and thickness of 0.6 mm, was polished with sandpapers and cleaned ultrasonically in isopropyl alcohol bath for 5 min. It was loaded into the PECVD system which was maintained at the base

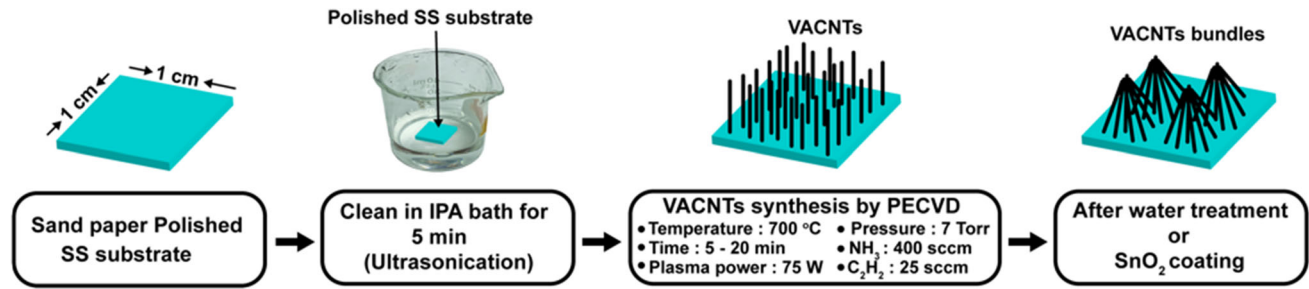


Figure 1 Schematic of the synthesis process for VACNTs on the SS substrate by PECVD method.

pressure of 0.01 Torr. Ammonia (NH_3) gas was introduced at a rate of 400 sccm, while the pressure of the PECVD chamber was kept at 7 Torr. Then, the SS substrate was heated to a temperature of 700 °C. Once the targeted temperature was achieved, a DC plasma was turned on and maintained at 75 W. Finally, acetylene (C_2H_2) gas was introduced at a rate of 25 sccm while keeping the chamber pressure at 7 Torr throughout the VACNTs growth period.

A simple wet-chemical method similar to that reported by Han and Zettl [27] was used to synthesize SnO_2 nanoparticles on the external surface of the CNTs to form core-shell structured composite material. The as-synthesized VACNTs array (not separated from original SS substrate) was treated with nitric acid (HNO_3 , 40%) at room temperature for 2 h to clean the surface of nanotubes and to create the oxygen-containing functional groups on the VACNT wall. A solution was prepared at room temperature by mixing 1 g of tin (II) chloride (SnCl_2 , 98%, anhydrous) in 80 mL of deionized water, and then 1.4 mL of hydrochloric acid (HCl , 38%) was added. Finally, the acid-treated VACNTs sample, first rinsed with deionized water, was submerged into the solution for different coating periods. The solution was stirred by the gentle flow of air through the solution continuously to facilitate the coating process. Once the sample was coated for the desired time period, it was taken out from the solution and dried at 95 °C for 15 min.

Morphology of the as-synthesized VACNTs array was characterized by a field emission scanning electron microscope (SEM, JOEL JSM-6330F). A transmission electron microscope (TEM, FEI Tecnai F30) equipped with energy-dispersive X-ray spectrometer (EDAX), which was operated at 300 kV, was used to characterize the nanostructure of the as-synthesized VACNTs and SnO_2 nanoparticles grown on the CNT wall. The FE characteristics of the samples were

tested in a diode configuration enclosed in a vacuum chamber. The VACNTs array deposited SS substrate was made cathode, whereas a solid cylindrical SS rod was used as an anode. The gap between the anode and cathode was maintained at 500 μm . All the experiments were performed at a vacuum level about 7×10^{-7} Torr. Keithley 236 SMU was used to measure the emission current from the VACNT emitters, whereas Matsusada AU-15P20 DC high voltage-power supply was used to supply the power during the experiments. Electrostatic field distribution for the VACNT emitters was simulated by using COMSOLTM MULTIPHYSICS 5.2 software. Three-dimensional (3D) models consisting of single VACNT, VACNTs array, and system having VACNTs bundles were created, as shown in Fig. 10. The parameters such as length of VACNT = 8 μm , the diameter of VACNT = 130 nm, and inter-VACNT distance = 0.3 μm were chosen to be reasonably close to the real VACNTs emitters system (20-min sample, as shown in Fig. 2c, f). An electric field of 1 V/ μm was applied between the top and bottom boundaries of the model. Surface and contour plots were used to visualize the results, whereas the magnitudes of local electric fields were recorded by using a point evaluation icon.

Results and discussion

Synthesis of VACNTs

SS sheet (304 type, Fe 72%, Cr 18%, Ni 8%, Mn 2% by wt.) received from Kimball Physics Inc. was first polished with sandpapers to remove a thin layer of chromium passive oxide (Cr_2O_3). This passive oxide layer is primarily used for the corrosion resistance purpose and is a weak catalyst for CNT growth [28]. A heat treatment at 700 °C to the polished SS substrate under an NH_3 environment helped to create

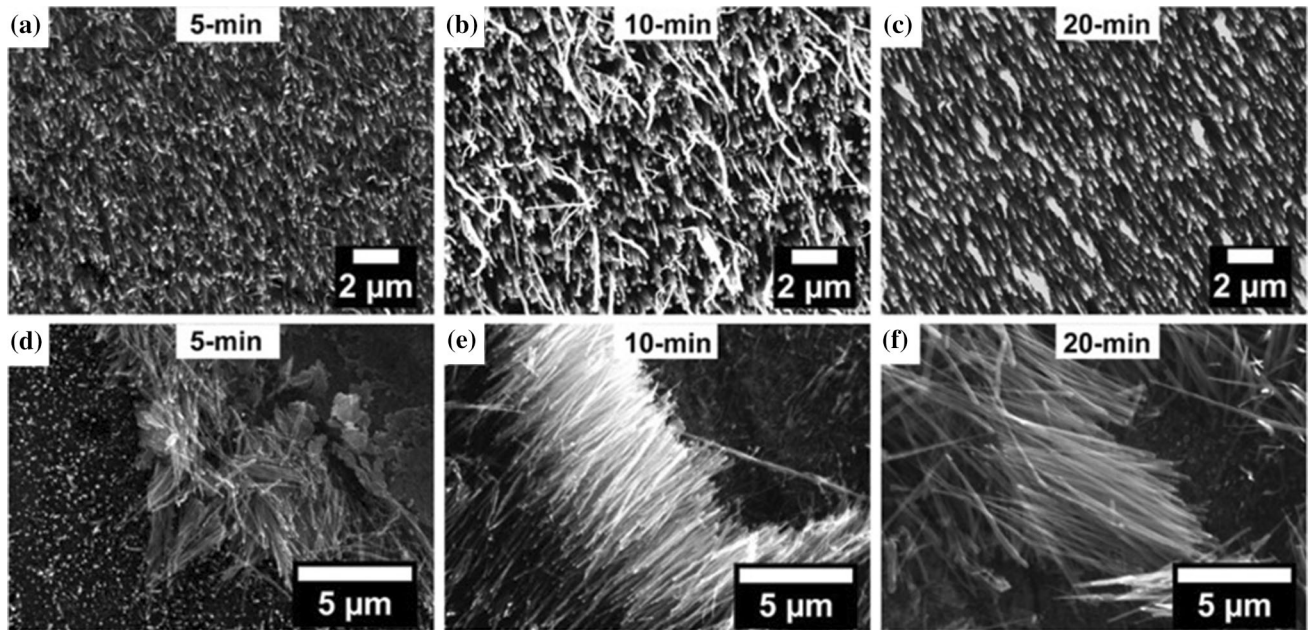


Figure 2 SEM images of CNTs (tilted view and corresponding scratched area) synthesized on SS for **a** 5 min, **b** 10 min, and **c** 20 min, respectively. The other growth parameters (growth temperature of 700 °C, flow of C₂H₂ at 25 sccm, flow of NH₃ at

400 sccm, pressure of 7 Torr and plasma power of 75 W) were kept constant throughout the synthesis process. **d–f** Corresponding scratched areas showing the length of the CNTs.

catalyst nano-hills [26] (such as Fe, Ni, or Mn which are the constituents of the substrate and are regarded as suitable catalysts for CNT growth) on the substrate surface. The on-site decomposition, diffusion into the active nucleation sites (nano-hills), and precipitation of the carbon atoms or clusters were the basis for the CNT formation. An energetic plasma of power 75 W aligned the CNTs in the direction parallel to the applied electric field (i.e., perpendicular to the substrate surface). The presence of the NH₃ gas ensured the etching of amorphous carbon deposited on the surface of the catalyst nanoparticles to keep them clean so that the diffusion and precipitation of carbon atoms or clusters could continue as the growth process continued.

Through a series of experiments, we optimized the VACNTs synthesis conditions which include a growth temperature of 700 °C, a flow rate of C₂H₂ at 25 sccm, a flow of NH₃ at 400 sccm, a pressure of 7 Torr, and a plasma power of 75 W [26]. In this report, we synthesized the VACNTs for the growth time in the range of 5 to 20 min by keeping other growth parameters constant to obtain the VACNTs with different length. Figure 2 shows typical SEM images of CNTs where Fig. 2a–c represents images tilted at 15° to the normal of the SS substrate, and

Fig. 2d–f represents their corresponding scratched area where CNTs length was measured. It was observed that the average length of the CNTs was 2.13 μm (standard deviation, $w = 0.23$ μm), 4.13 μm ($w = 0.68$ μm), and 8.15 μm ($w = 1.03$ μm) at growth times of 5, 10, and 20 min, respectively. Thus, a linear relationship between the CNT's length and growth time was observed, which was in good agreement with our prediction. Also, the average diameter of the CNTs was found to be 138.17 nm ($w = 24.51$ nm), 139.70 nm ($w = 28.29$ nm), and 132.07 nm ($w = 33.35$ nm) for the samples grown for 5 min (5-min sample), 10 min (10-min sample), and 20 min (20-min sample), respectively. We performed our experiments in the growth time range 5 to 20 min since an extended growth time (> 20 min) slowed down the growth rate of the CNTs. This is because the catalyst particles eventually lost their catalytic activity as the growth time increased [29]. Moreover, prolonged exposure of the VACNTs to the intense plasma may also destroy the graphitization of the VACNTs giving rise to wall defects which can hinder the desired longer FE stability of VACNT emitters. These results imply that growth time had a significant effect on the CNTs length while synthesizing them by the PECVD method.

The nanostructure of the as-synthesized CNTs was characterized by low and high-resolution TEM images. Figure 3a represents the low-resolution TEM image of CNTs synthesized for 10 min. It is evident from the TEM image that a catalyst particle was encapsulated at the tip of each individual CNTs suggesting the tip growth model. The diameter variation among the CNTs, as shown in Fig. 3a, was determined by the size of the catalyst particles anchored at the tip of CNTs. These catalyst particles were the catalyst nano-hills formed on the SS substrate, and they were lifted off the SS substrate by the growing CNTs. Figure 3b represents a high-resolution TEM image of the CNT, which shows that the graphitic planes are not parallel to the tube axis but twisted to form a stacked-cup structure resembling a bamboo-like morphology. This kind of growth pattern is a common characteristic of the CNTs grown by PECVD [30, 31]. The inset in Fig. 3b is a close-up view of the boxed area of the CNT wall shown in Figure, and it shows the twisted graphene layers forming the bamboo-like structure. The distance between the adjacent graphene layers is 0.34 nm, which corresponds to the (002) graphitic plane. It is believed that nitrogen atoms incorporated into the graphene layers (CNT walls) during the synthesis process by pyrrolic-like nitrogen binding configuration (sp^3 hybridization) played a vital role in the formation of the bamboo-like CNTs [32]. The sp^3 hybridized nitrogen atoms form five-member rings together with carbon atoms of the graphene layer, which help to twist the graphene layer [33]. In our study, we used NH_3

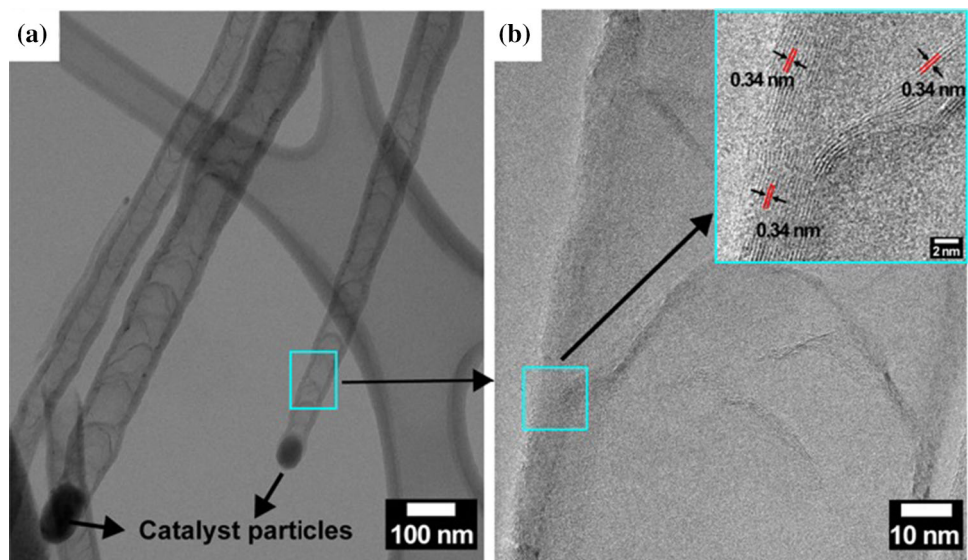
plasma during the VACNTs synthesis experiment, and a significant number of energetic nitrogen atoms can be doped into the graphene layers. The substitutional nitrogen atoms caused the formation of pentagons along with the regular hexagons leading to the formation of bamboo-like CNT morphology, as shown in TEM micrographs.

Water treatment to VACNT arrays

It has been reported that the treatment of the self-standing high-density VACNTs array with a volatile liquid helps to change the morphology of the array into individual bundles under the surface tension forces during drying process [34, 35]. Such a particular morphology can enhance the FE properties of VACNTs owing to their extended inter-bundle distance and the emission from the bundle as a whole [36]. It is important to mention that bundling phenomenon can provide a platform to achieve maximum FE via minimizing charge screening effects from the surrounding VACNTs in a dense array. To form bundled morphology, the as-synthesized VACNTs arrays were submerged into deionized water (80 mL) for 9 h at room temperature.

The water treatment was facilitated by a gentle flow of air through the deionized water. Once the treatment time was achieved, the samples were dried by using a hot plate at 95 °C for 15 min. As a result, self-assembled tapered bundles of VACNTs were achieved, as shown in Fig. 4. This change in morphology of the VACNTs array was attributed to the

Figure 3 TEM images of the CNTs synthesized on SS substrate at 700 °C for 10 min. **a** Low-resolution TEM image of CNTs with catalyst particles at the tip. **b** High-resolution TEM image showing CNT with “bamboo-like” structure. The inset in **(b)** represents a close-up view of the CNT wall showing the twisted graphitic layers.



surface tension of the deionized water which caused the van der Waals forces between the deionized water and the VACNTs to pull the tip of VACNTs to each other while the roots remained attached on the substrate during the drying process [37]. However, this effect was not clearly noticeable in the case of shorter VACNTs (Fig. 4a) as they were robust enough to counter the surface tension forces; but still, the bundled structures were present to some extent. It should be pointed out that the 9-h treatment to the VACNTs array to form bundles was not strictly necessary, and the desired morphology could be accomplished within a few minutes treatment. However, the treatment was performed for 9 h to be consistent with the SnO₂ coating time on VACNTs so that the FE properties of the two different samples can be compared. The average inter-bundle distance was measured as about 3 μm for the 20-min sample, which was significantly larger than the distance between individual self-standing VACNTs of the as-synthesized samples. Apart from bundling, the water treatment might also be able to remove amorphous carbon deposited on the surface of the sample during the PECVD growth process. This cleaning process could be beneficial in the case of FE applications of VACNTs which will be discussed later.

Coating VACNT arrays with SnO₂ nanoparticles

The as-synthesized VACNTs arrays were coated with SnO₂ nanoparticles by using a facile wet-chemical method for different time durations such as 9 and 11 h to understand the effect of coating time on SnO₂ nanoparticle size and coating thickness. The vertical alignment of the CNTs was significantly disturbed after the solution-based SnO₂ coating process as

compared to their pristine counterparts (i.e., the as-synthesized VACNTs arrays). Figure 5 shows the structure change of the VACNTs arrays after the SnO₂ coating process for 9 h, the original vertically standing CNTs formed cone-like bundles as the tip of CNTs was attached to each other. The bundling pattern was similar to that observed for water treatment, as shown in Fig. 4. This bundling phenomenon was clearly presented for longer CNTs, as shown in Fig. 5b, c, whereas it was not quite significant for shorter CNTs, as shown in Fig. 5a.

High- and low-resolution TEM images were used to study the distribution and morphology of the SnO₂ nanoparticles coated for 9 and 11 h on the surface of the CNTs. Figure 6 shows TEM images of the 10-min sample after coating with SnO₂ nanoparticles for 9 h. It is clear from the TEM images that all the CNTs were thoroughly coated with SnO₂ nanoparticles forming a CNT/SnO₂ core-shell structure. Figure 6a represents a low-resolution TEM image of the CNT/SnO₂ bundle, whereas Fig. 6b depicts a magnified view of a CNT/SnO₂ composite showing a coating layer of SnO₂ nanoparticles on the wall of the CNT. The high-resolution TEM image, as shown in Fig. 6c, shows the individual crystalline SnO₂ nanoparticles deposited on the exterior of the CNT's wall. The average thickness of the coating was about 10 nm. The inset on the top right corner of Fig. 6c displays a typical SnO₂ nanoparticle showing clear lattice fringes separated by a distance of 0.334 nm, which corresponds to the (110) lattice plane of the tetragonal SnO₂ crystal [27]. Also, the inset at the bottom right corner of Fig. 6c represents the selected area diffraction (SAED) pattern from the CNT/SnO₂ composite. The distinct concentric rings were indexed as (110), (101), (211), and (301) corresponding to the tetragonal phases of polycrystalline SnO₂ nanoparticles. The

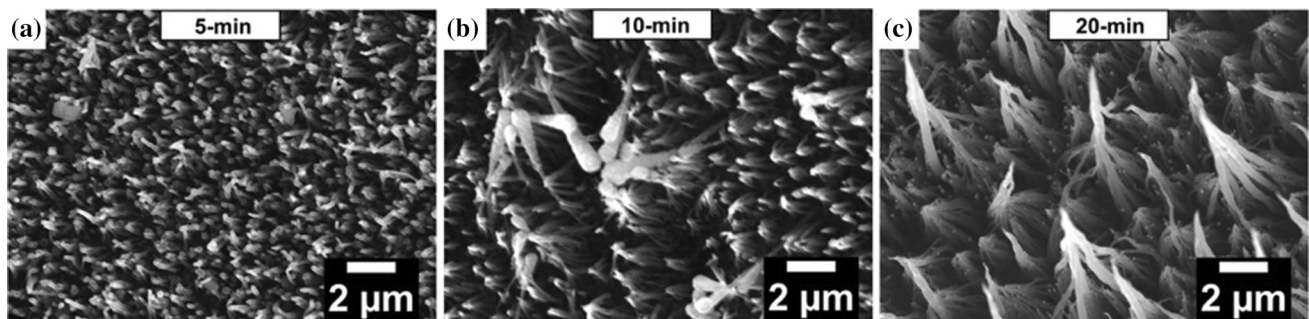


Figure 4 SEM images of **a** 5-min, **b** 10-min, and **c** 20-min sample showing bundling of VACNTs due to surface tension during the drying process after treating with water for 9 h.

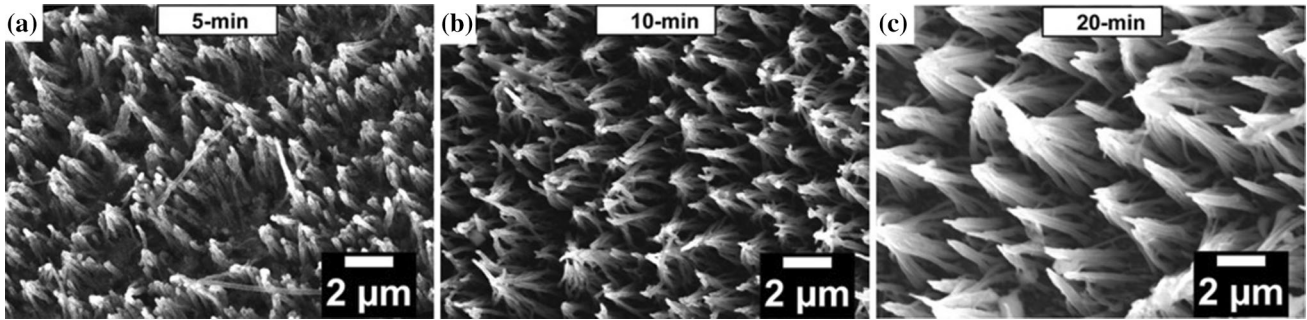


Figure 5 SEM images of **a** 5-min, **b** 10-min, and **c** 20-min sample showing conical bundle-like morphology of VACNTs after coating with SnO₂ nanoparticles for 9 h.

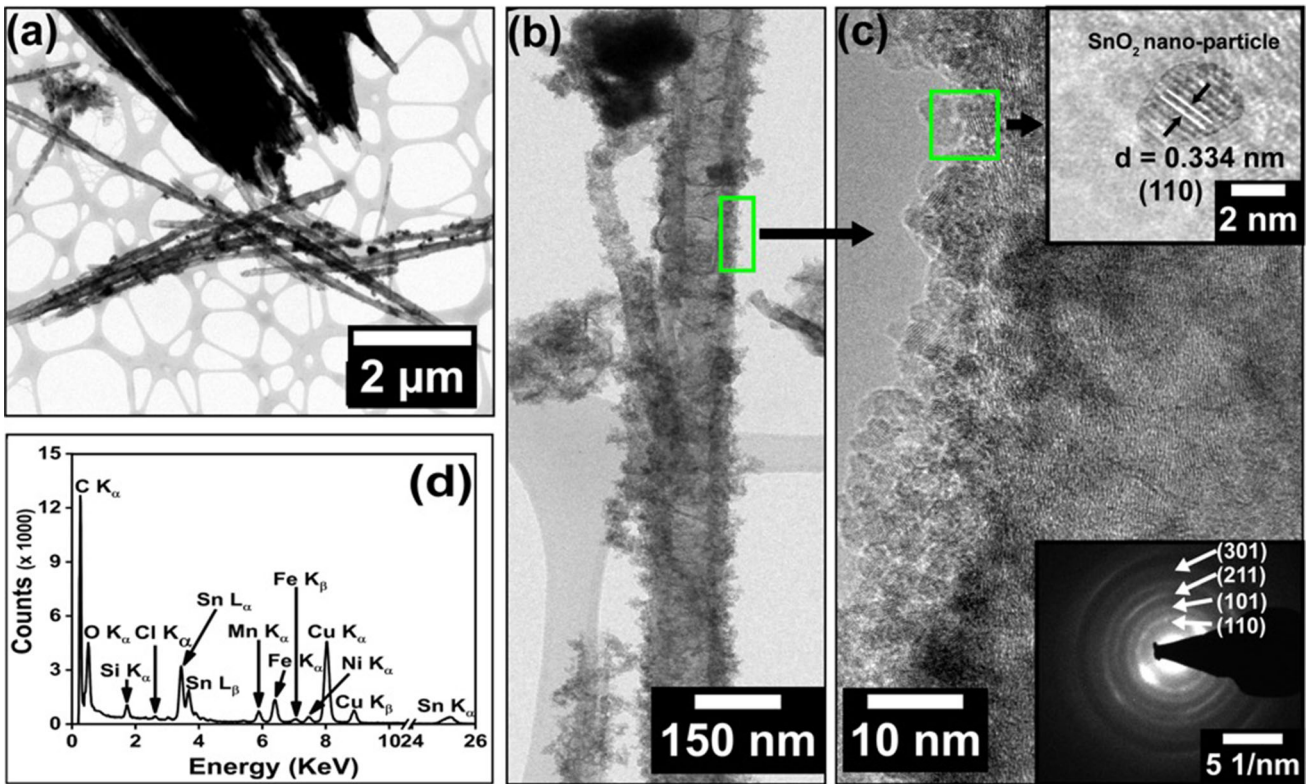


Figure 6 TEM images of the SnO₂ nanoparticles coated for 9 h on the surface of CNTs grown for 10 min **a** Low-resolution TEM image of CNT/SnO₂ bundle, **b** Magnified view of SnO₂-coated CNT showing the SnO₂ coating layer on the CNT surface **c** Close-up view of the boxed area indicated in **(b)**, showing clearly the individual SnO₂ nanoparticles deposited on the CNT surface. The inset on the top right side of **(c)** represents a high-resolution TEM

image of a SnO₂ nanoparticle showing clear lattice fringes separated by a distance of 0.334 nm which corresponds to the (110) lattice plane of the SnO₂ crystal. The inset on the bottom right corner of **(c)** represents a SAED pattern showing the polycrystalline nature of SnO₂ nanoparticles layer. **d** EDAX spectrum showing the composition of CNT/SnO₂ composite.

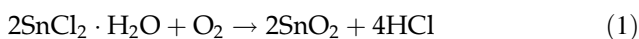
presence of Sn and O in the EDAX spectrum, as shown in Fig. 6d, further confirmed the presence of polycrystalline SnO₂ nanoparticles. However, the chemical analysis using EDAX showed the presence of other elements such as C, Si, Fe, Mn, Ni, and Cu besides Sn and O in the coated multiwalled CNT. The

C signal was due to the multiwalled CNT, whereas a weak signal of Si could be from the following two sources: (1) contamination of the glass beaker as a result of reaction with the HNO₃ during the pre-treatment of CNTs or (2) interaction of the strong C signal and Al, which is part of the collimator [38]. The

strong Cu signal was from the TEM grid, whereas the weak signals of Fe, Mn, and Ni were expected from the SS substrate or the catalyst particles responsible for the CNTs growth.

Figure 7a, b represents the distribution of the diameter of SnO₂ nanoparticles synthesized for 9 and 11 h, respectively. The histograms were created after a representative number of SnO₂ particles from the samples were counted. Based on the diameter histogram, it was observed that the average SnO₂ particle size increased with the increasing coating time. The average diameter (x_c) of the SnO₂ particles for 9 h coated sample was found to be 4.18 nm with standard deviation (w) of 0.17 nm, as shown in Fig. 7a. More than 90% of the particle's diameters were found to be in the range from 3 to 5.5 nm. Similarly, as shown in Fig. 7b, the average diameter (x_c) of the SnO₂ particles for 11 h coated sample was found to be 5.86 nm with the standard deviation (w) of 0.16 nm and more than 90% of the particle's diameters were observed to be in the range from 5 to 7.5 nm.

The as-synthesized multiwalled CNTs were treated with HNO₃ before coating SnO₂ nanoparticles on the CNTs surface in order to create carboxyl or hydroxyl functional groups. The hydrophilic functional groups are essential in achieving a uniform SnO₂ coating over the length of the CNTs [39]. The synthesis of ultra-fine SnO₂ nanoparticles from an aqueous solution of SnCl₂ precursor can be accredited to the following chemical reaction: [27]



In brief, the mechanism of SnO₂ phase formation and coating on the wall of CNT can be understood as follows. First, Sn²⁺ cations present in the precursor SnCl₂ aqueous solution were adsorbed on the negatively charged functional groups on the CNT surface due to electrostatic interaction [40]. Then, the Sn²⁺ cations were oxidized to form SnO₂ nanoparticles in the presence of oxygen in the solution. Here, the addition of a small amount of HCl in the precursor SnCl₂ aqueous solution was very crucial because it prevented the formation of tetratin hexhydroxide dichloride (Sn₄(OH)₆Cl₂) colloidal particles as a result of hydrolysis of SnCl₂ which would eventually lead to the formation of SnO instead of SnO₂ nanoparticles [41].

Field emission (FE) properties measurement

A schematic to measure the FE properties of the VACNTs in diode configuration is shown in the inset of Fig. 8a. A stainless steel (SS) plate was used as a cathode, whereas a solid cylindrical SS rod (0.803 cm², surface area facing VACNTs) was used as an anode. Silver (Ag) paste was used to attach the sample onto the SS cathode as it is an excellent electrical conductor. During the experiment, the emission current was measured as the applied voltage was systematically increased in steps of 50 V until the emission current was saturated. For practical application and comparison purpose of the measured data, we define turn-on electric field (E_{TO}) and threshold electric field (E_{TH}) as the electric field required to produce the emission current densities of 1 μA/cm² and 1 mA/cm², respectively. The field

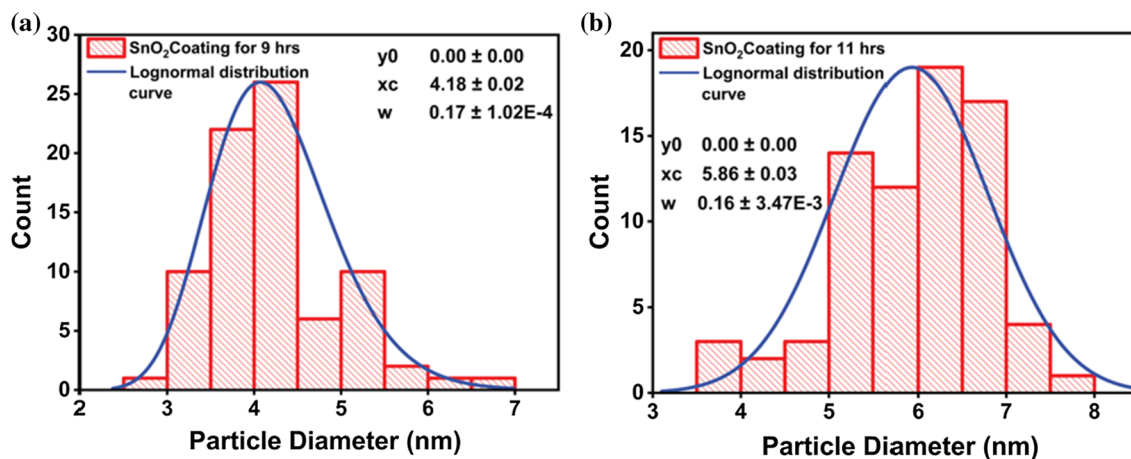


Figure 7 Particle size distribution of SnO₂ nanoparticles coated for a 9 h and b 11 h, on the surface of CNTs grown for 10 min.

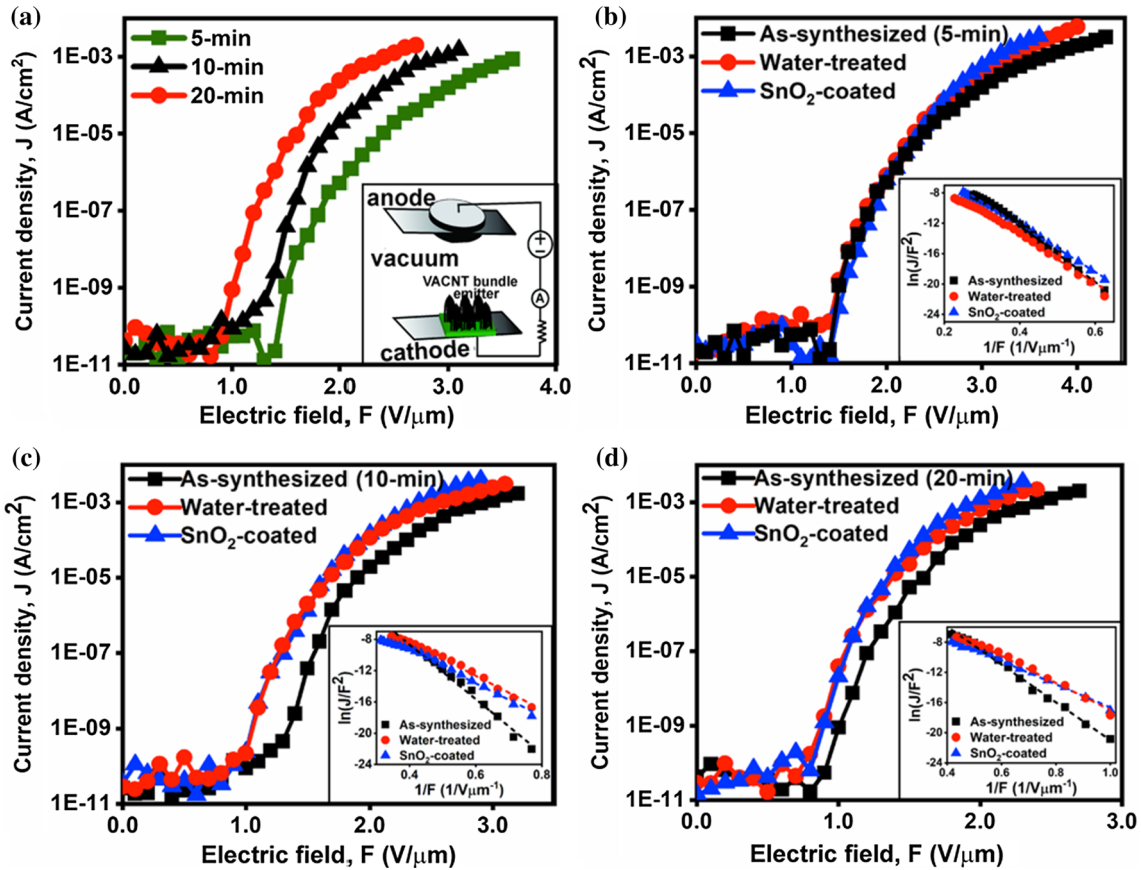


Figure 8 FE characteristics of as-synthesized, water-treated, and SnO₂-coated VACNTs. **a** Emission current density versus applied electric field (F–J plot) for the as-synthesized VACNTs grown for 5 min, 10 min, and 20 min. The inset shows the schematic

enhancement factor (β) was studied by using the Fowler–Nordheim (F–N) equation [42]:

$$J = \left(\frac{\beta^2 A F^2}{\phi} \right) \exp \left(\frac{B \phi^3}{\beta F} \right) \quad (2)$$

where J is the emission current density, $A = 1.56 \times 10^{-6} \text{ A V}^{-2} \text{ eV}$ and $B = 6.83 \times 10^9 \text{ eV}^{-3/2} \text{ V m}^{-1}$ [43, 44] are Fowler–Nordheim constants, ϕ is the work function of the field emitter, and F is the applied electric field. It has been reported that the tip work function varies slightly for metallic (4.6 eV) and semiconducting (5.6 eV) CNTs, depending upon their helicity [45]. Different helicities and slight variation in the work function were expected in a dense mat of VACNTs array. Hence, the work function of the CNT emitter was assumed to be 5.0 eV (work function of carbon) [46] and the field enhancement factors were calculated by using the

diagram of the FE measurement setup. Comparative F–J plots for as-synthesized, water-treated, and SnO₂-coated VACNTs samples synthesized for **b** 5 min, **c** 10 min, and **d** 20 min, respectively. The insets are their corresponding Fowler–Nordheim (F–N) plots.

slopes of the fitted F–N plots, i.e., graph of $\ln(J/F^2)$ versus $1/F$, as shown in the insets of Fig. 8b–d.

The FE properties of the various samples are presented in Table 1. Figure 8a represents the plot of emission current density versus applied electric field (F–J plot) of three pristine VACNTs samples with different average lengths. The samples demonstrated different FE characteristics according to their lengths. The E_{TO} for shorter VACNTs such as 5-min sample was observed to be 2.14 V/ μm , and its E_{TH} was found to be 3.53 V/ μm . The E_{TO} for longer VACNTs such as 10-min and 20-min sample was 1.68 and 1.40 V/ μm , respectively, whereas their E_{TH} 's were recorded as 3.00 and 2.31 V/ μm , respectively. As the average length of the VACNTs was increased, better FE performance (i.e., lower values of E_{TO} and E_{TH}) was observed, as shown in Fig. 8a. Also, the field enhancement factor (β) for pristine 5-min, 10-min, and 20-min samples was calculated as 2357, 2668, and

Table 1 FE properties of as-synthesized, water-treated, and SnO₂ coated VACNTs

Sample	Before stability test			After stability test		
	E_{TO} (V/ μ m)	E_{TH} (V/ μ m)	β	E_{TO} (V/ μ m)	E_{TH} (V/ μ m)	β
5-min						
As-synthesized	2.14	3.53	2357	2.35	3.85	1991
Water-treated	2.12	3.39	2449	2.37	3.90	2044
SnO ₂ -coated	2.12	3.30	2486	2.34	3.80	2015
10-min						
As-synthesized	1.68	3.00	2668	1.83	3.26	2359
Water-treated	1.45	2.58	3391	1.65	2.61	2818
SnO ₂ -coated	1.43	2.50	3451	1.62	2.58	2826
20-min						
As-synthesized	1.40	2.31	3046	1.64	2.74	2979
Water-treated	1.19	2.20	4670	1.41	2.65	4020
SnO ₂ -coated	1.18	2.01	4712	1.37	2.58	4109

3046, respectively. The straight lines seen in the F–N plots (insets of Fig. 8b–d) indicate that the observed FE phenomenon was mainly due to the quantum mechanical tunneling process [47]. The geometrical field enhancement factor (β') of an individual CNT emitter can be estimated by the ratio of the length to radius of the CNT [12]. In our case, the average radius of the VACNTs for the aforementioned three samples was similar, and therefore, the length was the only critical factor which can affect the β' . The increased β values for the longer VACNTs agree with the geometrical β' estimation. However, the large inconsistency in the experimental and geometrical beta values (e.g., $\beta \approx 3046$ and $\beta' \approx 107$ for 20-min sample) suggests that the quantum tunneling was not the sole mechanism responsible for the observed FE performance. The tip of the carbon nanotubes may not only be the area where the field emission process occurs. Chhowalla et al. [48] suggested that in the case of diode configuration method, a triple junction between the substrate, base of the CNTs, and vacuum can force the electrons to be emitted to the vacuum.

Figure 8b–d shows the F–J plots for the pristine, water-treated, and SnO₂-coated VACNTs synthesized for 5, 10, and 20 min, respectively. The insets are their corresponding F–N plots. In the case of 5-min samples, the E_{TO} values were reasonably similar; however, the E_{TH} values were improved (decreased) as the pristine samples were treated with water and coated with SnO₂ nanoparticles. Further, the field enhancement factors were calculated as 2357, 2449, and 2486 for pristine, water-treated, and SnO₂-coated samples, respectively. For longer VACNTs, such as

10 and 20-min samples, significant improvement in the FE performance was observed after the post-treatments to the as-synthesized VACNTs arrays, as shown in Fig. 8c, d. For example, the E_{TO} for the as-synthesized 10-min sample was 1.68 V/ μ m, which was lowered to 1.45 and 1.43 V/ μ m for the water-treated and SnO₂-coated samples, respectively. The E_{TH} was also improved after the post-treatments; the values were measured to be 3.00, 2.58, and 2.50 V/ μ m for as-synthesized, water-treated, and SnO₂-coated samples, respectively. Furthermore, the field enhancement factor was increased considerably after the post-treatments, and the values were 2668, 3391, and 3451 for the as-synthesized, water-treated, and SnO₂-coated samples, respectively. A very similar trend of FE performance to that of the 10-min samples was observed for the 20-min samples, as shown in Fig. 8d. The lowest $E_{TO} = 1.18$ V/ μ m, $E_{TH} = 2.01$ V/ μ m, and the highest $\beta = 4712$ among all the samples along with the maximum emission current density of about 7 mA/cm² at 2.50 V/ μ m were recorded for the SnO₂-coated 20-min sample.

These results imply that the main reason for the enhanced FE performance from the post-treated samples was the restructuring of the morphology of the VACNTs array into individual sharp conical bundles, as shown in Fig. 4 and 5. The result also implies that a bundle emits as a whole rather than individual CNTs and the bundling alleviates the charge screening effect through increasing the distance between the effective emitters. For example, an inter-tube distance of about 0.3 μ m was measured in case of the pristine 20-min sample and after the water

treatment and SnO₂ coating, and the inter-bundle distance was measured to be about 3 μm. An optimum ratio of CNT height and inter-tube distance (l/s) has been suggested as 1.5:1 [13] or 1:2 [17] for a high field amplification. The l/s in our case was 2.7:1 (after the posttreatments to pristine 20-min sample) which is much close to the ideal ratio as compared to that for pristine sample (about 27:1). As a result, the field enhancement factor was improved significantly, and consequently, much lower values of E_{TO} and E_{TH} were observed in comparison with that for the pristine samples. Recently, Gupta et al. have reported low E_{TO} (0.6 V/μm at 1 μA/cm²) and E_{TH} (0.7 V/μm at 10 μA/cm²) from an array of VACNT-based square pillar of several millimeters high and 500 μm wide [16]. However, the total emission current density was rather low (4 mA/cm²) regarding the millimeter long VACNTs because the field emission came mainly from the edge rather than the tip of the flat pillar structured emitter. Wang et al. observed improved FE properties ($E_{TO} = 0.73$ V/μm at 10 μA/cm², $E_{TH} = 1.29$ V/μm at 10 mA/cm², and total emission current density of about 30 mA/cm²) from dense VACNT-based pillar structure (height 30 μm, diameter 20 μm, and $l/s = 1:2$) due to the minimum screening effect [17]. Hazra et al. reported extremely low E_{TO} (0.16 V/μm at 10 μA/cm²) and impressively high emission current density of about 1.5 A/cm² at 0.3 V/μm from the VACNT-based pillar structure of height 132 μm and base diameter 80 μm [15]. It is important to note that such an impressive result was possible only after the plasma treatment to the VACNT pillars to create an extremely sharp tip of the pillar structure (tip diameter < 1 μm). The reported results indicate that isolated VACNT pillars have much better FE performance than uniform VACNT arrays. Our research findings agree well with the reported results, and further, our method for converting uniform VACNTs array into bundled array is simple and efficient and can be easily applied to the large area of VACNTs array. Comparing some reported results in the above literatures, the FE performance of our bundled CNT arrays was not as good due to possibly the low height of the bundled CNT arrays and the smaller inter-bundle distance. We expect that the bundling of VACNTs array with low density and long length will further improve their FE performance.

It is also worthwhile to mention the behavior of the F–J curve for water-treated and SnO₂-coated (10 and

20-min) samples at the higher emission field region. At the higher applied electric field region (i.e., beyond the E_{TO}), the F–J curves for water-treated samples saturated faster than that for the SnO₂-coated samples. As a result, the lowest values of E_{TH} were observed for SnO₂-coated samples as compared to water-treated and pristine samples. The slower saturation of the F–J curves for the SnO₂-coated samples in comparison with that of the water-treated samples at the higher field region could be due to the protection against the structural failure of VACNT emitters by SnO₂ coating due to Joules heating during the emission process. We also performed the temporal measurement of the emission current density for pristine and posttreated 20-min samples. During the experiments, the voltage was applied in such a way that the initial emission current density of 1 mA/cm² was recorded for all the samples and then the applied voltage was kept constant meanwhile recording the emission current density for 40 h. The SnO₂-coated sample showed a stable emission current during the stability test period, indicating a superior FE stability among three samples, as shown in Fig. 9. The emission current density from the pristine and water-treated VACNTs arrays was degraded rapidly with time than that of the SnO₂-coated sample. The mechanism for the superior FE stability of the SnO₂-coated VACNTs emitter was similar to that of CNTs coated with a thin layer of wide band gap semiconducting material such as ZnO [49], RuO₂ [21], and TiO₂ [50]. The defective sites formed on the VACNTs due to the intense plasma bombardment during the PECVD growth process were responsible for the poor electron emission lifetime of the pristine and water-treated VACNTs

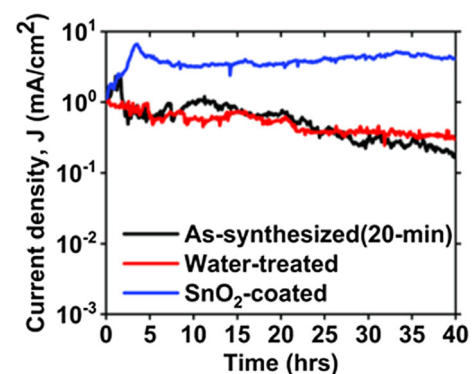


Figure 9 Stability comparison of the as-synthesized, water-treated, and SnO₂-coated VACNTs synthesized for 20 min.

arrays. In the case of SnO₂-coated VACNT emitters, however, the defects on the VACNTs were covered by the uniform SnO₂ layer. This SnO₂ layer protects the defective VACNTs from the destructive bombardment of energetic ions and radicals created in the emission process as well as residual oxygen molecules in the chamber. Also, it is to be noted that the FE performance from our samples even after electrical annealing (EA) for 40 h was not degraded significantly (see in Table 1). The consistency in the FE performance after the EA implies that there was no substantial change in the morphology of the bundled emitters which was further confirmed by the SEM images taken after the EA process (not shown in this report).

The CNT structure is made of *sp*² bonding between carbon atoms. The minimum energy required to remove a carbon atom from the structure is ~ 17 eV [51], and the melting point of CNTs is very high (~ 4800 K) [52]. Hence, it was tough to change the structure of CNTs, even at a large electric field. However, the eventual failure of the CNT emitters was inevitable at a certain electric field. Doytcheva et al. [53] performed an in situ TEM investigation on the structural failure in freestanding multiwalled CNTs and observed that CNTs suffered structural changes only after a certain current level but not gradually. Interestingly, they observed an increase in current level at a constant voltage followed by a shortening of the CNT due to tip failure, which resulted in a current drop. We also observed similar behavior in the emission current during the first few hours for SnO₂-coated sample, as shown in Fig. 9, where emission current was increased first and then decreased followed by a stable FE performance. Doytcheva et al. also suggested a critical current (i.e., a maximum current an individual CNT can withstand without undergoing structural failure) of 2–15 μA for CNTs with diameters in the range of 5–20 nm and a much higher critical current of 40–250 μA for CNTs with diameters about 30 nm. This means that the critical current for a CNT increases as the diameter increase. The average diameter of the VACNTs synthesized in our experiment was in the range of about 132–140 nm, and hence, they should be able to conduct high current without structural degradation. In addition, good contact between VACNTs and the substrate as well as an excellent thermal conductivity of CNTs and SS allowed an easy and sufficient transfer of the heat. This may help to prevent the

VACNTs from damage caused by Joule heating. Therefore, the excellent emission current stability for such a long period of time from our sample can be attributed to the lower thermal stress, high critical current, uniform local electric field for many emission sites (bundles), strong adhesion of VACNTs to the SS substrate, and coating of emitters by crystalline SnO₂ nanoparticles.

To further support our conclusions, we simulated the electrostatic field distribution for a single VACNT, an array of individual VACNTs, and bundled VACNTs with different number of VACNTs per bundle, as shown in Fig. 10. Figure 10a represents the electrostatic field distribution at the tip of a single VACNT, and the local electric field was found to be the strongest (about 455 V/μm) in comparison with other structures such as array and bundled structures. This result was obvious because there were no other VACNTs to affect via the screening effect. The presence of the strongest electric field was well supported by the fact that most field penetration occurred around the single VACNT emitter, as shown in Fig. 10a. In the case of VACNTs array (Fig. 10b), the local electric field at the tip of emitters was recorded as about 188 V/μm. This remarkable drop in the electric field strength was mainly due to the screening effect from the neighboring VACNTs in the closely packed array. The screening effect was evident from the weak penetration of the equipotential lines between the VACNT emitters, as shown in Fig. 10b. On the other hand, the local electric field was found to be 355 V/μm for the bundled structure with 9 VACNTs per bundle (Fig. 10c). It was about 89% increase in the local electric field strength as compared to that for the closely packed VACNTs array. This significant improvement in the local electrostatic field can be attributed to the increased inter-bundle distance (0.9 μm), which can lower the screening effect [36, 54].

We also simulated the local electric field distribution for the bundled structures having 17 VACNTs per bundle (not shown in this report) and 25 VACNTs per bundle (Fig. 10d) to study how the number of VACNTs in a bundle affects the FE process. The maximum local electric field (E_{\max}) versus emitter morphology is graphed in Fig. 11. The graph shows that a single VACNT has the highest local electric field, and the closely packed VACNTs array has the lowest local electric field. For VACNT bundles, the array with 9 VACNTs per bundle displayed

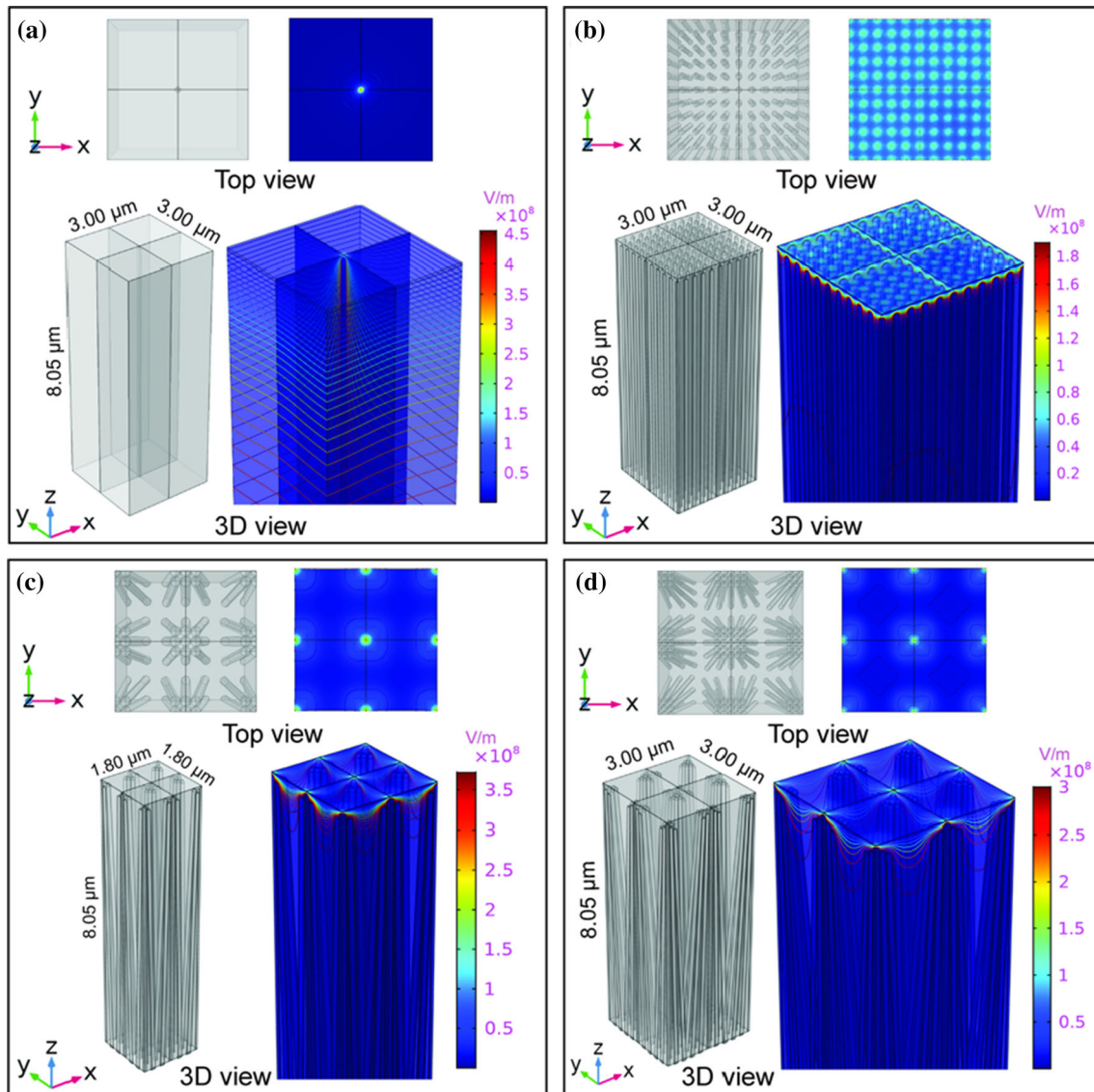


Figure 10 Electrostatic field distribution (simulation result) for **a** a single VACNT **b** an array of individual VACNTs, **c** bundled VACNTs with 9 VACNTs per bundle, and **d** bundled VACNTs with 25 VACNTs per bundle.

the highest local electric field, and the field decreased as the number of VACNTs in a bundle increased. Therefore, the simulation result suggests that the bundled field emitters with a smaller number of emitters per bundle (for example, 9 VACNTs/per bundle) can deliver better FE performance as compared to that from the dense emitters array and bundled emitters with a larger number of VACNTs per bundle. Our simulated result for pristine and posttreated VACNTs (bundled structures) agrees well with our experimental results. Our current experimental technique cannot control the number of VACNTs in a bundle, but the bundling through

simple water treatment and SnO₂ coating, as described in the report, can be a promising way to optimize the FE performance of VACNT arrays.

As the VACNTs were synthesized directly on the SS substrate without a buffer layer, the contact resistance between the substrate and CNTs was expected to be reduced substantially. The reduced contact resistance facilitated an easier electron transport in the interface between the substrate and the CNTs, through the CNTs, and finally emission into the vacuum, enhancing the overall FE performance. Also, the VACNTs synthesized by our method may be doped with nitrogen since an ammonia plasma

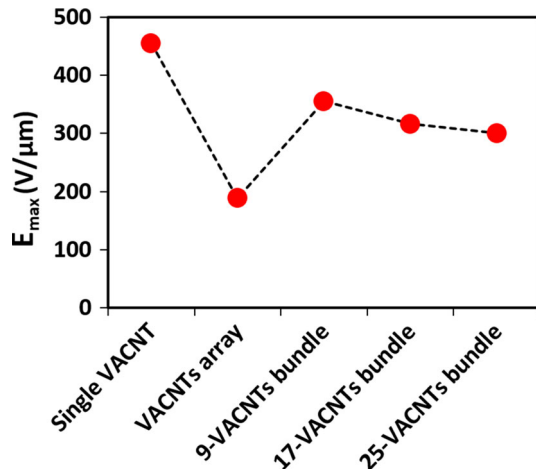


Figure 11 Change of electrostatic field as a function of emitter morphology (results are based on the simulation shown in Fig. 10).

was used during the experiment. Chen et al. [55] conducted an XPS N 1S spectra study on CNTs treated by the ammonia plasma and demonstrated the presence of a carbon–nitrogen bonding on the CNTs wall. They also revealed the occurrence of doped nitrogen even for an untreated CNTs as they used the ammonia plasma during the synthesis process. The nitrogen doping on the VACNTs was expected in our samples as we used ammonia plasma during the experiments. It has been reported that the FE properties of CNTs can be improved by the nitrogen doping [43]. Hence, the combined effects of low contact resistance between the substrate and the CNTs, highly conductive substrate, nitrogen-doped CNTs, bundled morphology, and SnO₂ coating greatly enhanced the FE properties of the multi-walled VACNTs synthesized on the SS substrate by PECVD.

Conclusions

In summary, VACNTs have been grown directly on SS substrate without adding extra buffer and catalyst layers on top of the substrate surface using the PECVD method. A linear dependency of VACNTs length on growth time was observed. The VACNTs were successfully coated with uniform layer of crystalline SnO₂ nanoparticles (average diameter of 4.18 nm for 9 h coating) by a facile wet-chemical method. The FE properties of VACNTs with different lengths were compared, and the longer VACNTs (20-

min sample) demonstrated better FE performance in terms of low turn-on electric field ($E_{\text{TO}} = 1.40 \text{ V}/\mu\text{m}$) and low threshold electric field ($E_{\text{TH}} = 2.31 \text{ V}/\mu\text{m}$) as well as higher field enhancement. This is because the longer VACNT resulted in a higher aspect ratio which in turn leads to the greater field enhancement. The posttreatment to the pristine VACNTs samples such as water treatment and SnO₂ nanoparticles coating significantly enhanced the FE properties (the E_{TO} and E_{TH} were 1.18 and 2.01 V/ μm , respectively, for SnO₂-coated 20-min sample) due to the structural change which greatly reduced the screening effect. The effect of bundling of VACNTs on the local electric field was simulated, and the experimental and simulation results agree well. Longer VACNTs coated with SnO₂ nanoparticles presented superior FE stability among all the tested samples. The superior FE stability can be attributed to the mechanical strength enhancement and chemical stability of the VACNT emitters. The present method of direct synthesis of VACNTs arrays on the conductive substrate such as stainless steel and their structural modification through water treatment and SnO₂ nanoparticles coating can be potentially useful in the field emission devices that require low bias and longer emission current stability.

Acknowledgements

This work is supported by the National Science Foundation under grant DMR-1506640. This work was performed, in part, at the Center for Integrated Nanotechnologies, an Office of Science User Facility operated for the US Department of Energy (DOE) Office of Science. Sandia National Laboratories is a multi-mission laboratory managed and operated by National Technology and Engineering Solutions of Sandia, LLC., a wholly owned subsidiary of Honeywell International, Inc., for the US DOE's National Nuclear Security Administration under contract DE-NA-0003525. This paper describes objective technical results and analysis. Any subjective views or opinions that might be expressed in the paper do not necessarily represent the views of the US Department of Energy or the US Government. The authors would also like to acknowledge the support from Advanced Materials Engineering Research Institutes (AMERI) at Florida International University.

Compliance with ethical standards

Conflict of interest The authors declare that they have no conflict of interest.

References

- [1] Qian D, Wagner GJ, Liu WK, Yu MF, Ruoff RS (2002) Mechanics of carbon nanotubes. *Appl Mech Rev* 55(6):495–533
- [2] Hone J, Llaguno MC, Biercuk MJ, Johnson AT, Batlogg B, Benes Z et al (2002) Thermal properties of carbon nanotubes and nanotube-based materials. *Appl Phys A Mater Sci Process* 74(3):339–343
- [3] Bockrath M, Cobden DH, McEuen PL, Chopra NG, Zettl A, Thess A et al (1997) Single-electron transport in ropes of carbon nanotubes. *Science* 275(5308):1922–1925
- [4] Poudel YR, Li W (2018) Synthesis, properties, and applications of carbon nanotubes filled with foreign materials: a review. *Mater Today Phys* 7:7–34
- [5] Choi WB, Chung DS, Kang JH, Kim HY, Jin YW, Han IT et al (1999) Fully sealed, high-brightness carbon-nanotube field-emission display. *Appl Phys Lett* 75(20):3129–3131
- [6] Baughman RH, Zakhidov AA, De Heer WA (2002) Carbon nanotubes—the route toward applications. *Science* 297(5582):787–792
- [7] Yue GZ, Qiu Q, Gao B, Cheng Y, Zhang J, Shimoda H et al (2002) Generation of continuous and pulsed diagnostic imaging x-ray radiation using a carbon-nanotube-based field-emission cathode. *Appl Phys Lett* 81(2):355–357
- [8] Milne WI, Teo KBK, Minoux E, Groening O, Gangloff L, Hudanski L et al (2006) Aligned carbon nanotubes/fibers for applications in vacuum microwave amplifiers. *J Vacuum Sci Technol B Microelectron Nanometer Struct* 24(1):345–348
- [9] Li J, Papadopoulos C, Xu J (1999) Growing Y-junction carbon nanotubes. *Nature* 402:253–254
- [10] Morassutto M, Tiggelaar RM, Smithers M, Gardeniers JG (2016) Vertically aligned carbon nanotube field emitter arrays with Ohmic base contact to silicon by Fe-catalyzed chemical vapor deposition. *Mater Today Commun* 7:89–100
- [11] Talapatra S, Kar S, Pal SK, Vajtai R, Ci L, Victor P et al (2006) Direct growth of aligned carbon nanotubes on bulk metals. *Nat Nanotechnol* 1(2):112–116
- [12] Neupane S, Yang Y, Li W, Gao Y (2014) Synthesis and enhanced electron field emission of vertically aligned carbon nanotubes grown on stainless steel substrate. *J Nanosci Lett* 4:14–20
- [13] Bonard JM, Weiss N, Kind H, Stöckli T, Forró L, Kern K, Chatelain A (2001) Tuning the field emission properties of patterned carbon nanotube films. *Adv Mater* 13(3):184–188
- [14] Kim D, Lim SH, Guilley AJ, Cojocaru CS, Bourée JE, Vila L et al (2008) Growth of vertically aligned arrays of carbon nanotubes for high field emission. *Thin Solid Films* 516(5):706–709
- [15] Hazra KS, Rai P, Mohapatra DR, Kulshrestha N, Bajpai R, Roy S et al (2009) Dramatic enhancement of the emission current density from carbon nanotube based nanosize tips with extremely low onset fields. *ACS Nano* 3(9):2617–2622
- [16] Gupta BK, Kedawat G, Gangwar AK, Nagpal K, Kashyap PK, Srivastava S et al (2018) High-performance field emission device utilizing vertically aligned carbon nanotubes-based pillar architectures. *AIP Adv* 8(1):015117
- [17] Wang K-Y, Liao C-Y, Cheng H-C (2016) Field-emission characteristics of the densified carbon nanotube pillars array. *ECS J Solid State Sci Technol* 5(9):M99–M103
- [18] Li Z, Yang X, He F, Bai B, Zhou H, Li C et al (2015) High current field emission from individual non-linear resistor ballasted carbon nanotube cluster array. *Carbon* 89:1–7
- [19] Li X, Niu J, Zhang J, Li H, Liu Z (2003) Labeling the defects of single-walled carbon nanotubes using titanium dioxide nanoparticles. *J Phys Chem B* 107:2453–2458
- [20] Green JM, Dong L, Gutu T, Jiao J, Conley JF, Ono Y (2006) ZnO-nanoparticle-coated carbon nanotubes demonstrating enhanced electron field-emission properties. *J Appl Phys* 99(9):1–4
- [21] Chen C-A, Lee K-Y, Chen Y-M, Chi J-G, Lin S-S, Huang Y-S (2010) Field emission properties of RuO₂ thin film coated on carbon nanotubes. *Vacuum* 84(12):1427–1429
- [22] Chakrabarti S, Pan L, Tanaka H, Hokushin S, Nakayama Y (2007) Stable field emission property of patterned MgO coated carbon nanotube arrays. *Jpn J Appl Phys* 46(7R):4364–4369
- [23] Sreekanth M, Ghosh S, Barman SR, Sadhukhan P, Srivastava P (2018) Field emission properties of indium-decorated vertically aligned carbon nanotubes: an interplay between type of hybridization, density of states and metal thickness. *Appl Phys A* 124(8):528–536
- [24] Sridhar S, Tiwary C, Vinod S, Taha-Tijerina JJ, Sridhar S, Kalaga K et al (2014) Field emission with ultralow turn on voltage from metal decorated carbon nanotubes. *ACS Nano* 8(8):7763–7770
- [25] Suriani A, Dalila A, Mohamed A, Mamat M, Malek M, Soga T et al (2016) Fabrication of vertically aligned carbon nanotubes–zinc oxide nanocomposites and their field electron emission enhancement. *Mater Des* 90:185–195
- [26] Thapa A, Neupane S, Guo R, Jungjohann KL, Pete D, Li W (2018) Direct growth of vertically aligned carbon nanotubes

- on stainless steel by plasma enhanced chemical vapor deposition. *Diam Relat Mater* 90:144–153
- [27] Han W-Q, Zettl A (2003) Coating single-walled carbon nanotubes with tin oxide. *Nano Lett* 3(5):681–683
- [28] Masarapu C, Wei B (2007) Direct growth of aligned multi-walled carbon nanotubes on treated stainless steel substrates 23(17):9046–9049
- [29] Bower C, Zhou O, Zhu W, Werder DJ, Jin S (2000) Nucleation and growth of carbon nanotubes by microwave plasma chemical vapor deposition. *Appl Phys Lett* 77(17):2767–2769
- [30] Chhowalla M, Teo KBK, Ducati C, Rupesinghe NL, Amaratunga GAJ, Ferrari AC et al (2001) Growth process conditions of vertically aligned carbon nanotubes using plasma enhanced chemical vapor deposition. *J Appl Phys* 90(10):5308–5317
- [31] Abadi PPSS, Maschmann MR, Hodson SL, Fisher TS, Baur JW, Graham S et al (2017) Mechanical behavior of carbon nanotube forests grown with plasma enhanced chemical vapor deposition: pristine and conformally coated. *J Eng Mater Technol* 139(3):034502
- [32] Arjmand M, Chizari K, Krause B, Pötschke P, Sundararaj U (2016) Effect of synthesis catalyst on structure of nitrogen-doped carbon nanotubes and electrical conductivity and electromagnetic interference shielding of their polymeric nanocomposites. *Carbon* 98:358–372
- [33] Jang JW, Lee CE, Lyu SC, Lee TJ, Lee CJ (2004) Structural study of nitrogen-doping effects in bamboo-shaped multi-walled carbon nanotubes. *Appl Phys Lett* 84(15):2877–2879
- [34] Lau KK, Bico J, Teo KB, Chhowalla M, Amaratunga GA, Milne WI et al (2003) Superhydrophobic carbon nanotube forests. *Nano Lett* 3(12):1701–1705
- [35] Mashayekhi A, Hosseini SM, Amiri MH, Namdar N, Sanaee Z (2016) Plasma-assisted nitrogen doping of VACNTs for efficiently enhancing the supercapacitor performance. *J Nanopart Res* 18(6):154–168
- [36] Pandey A, Prasad A, Moscatello J, Ulmen B, Yap YK (2010) Enhanced field emission stability and density produced by conical bundles of catalyst-free carbon nanotubes. *Carbon* 48(1):287–292
- [37] Zhang K, Li T, Ling L, Lu H, Tang L, Li C et al (2017) Facile synthesis of high density carbon nanotube array by a deposition-growth-densification process. *Carbon* 114:435–440
- [38] Rudloff-Grund J, Brenker F, Marquardt K, Kaminsky F, Schreiber A (2016) STEM EDX nitrogen mapping of nanoinclusions in milky diamonds from Juina, Brazil, using a windowless silicon drift detector system. *Anal Chem* 88(11):5804–5808
- [39] Barros E, Souza Filho A, Lemos V, Mendes Filho J, Fagan SB, Herbst M et al (2005) Charge transfer effects in acid treated single-wall carbon nanotubes. *Carbon* 43(12):2495–2500
- [40] Wang Z, Chen G, Xia D (2008) Coating of multi-walled carbon nanotube with SnO₂ films of controlled thickness and its application for Li-ion battery. *J Power Sources* 184(2):432–436
- [41] Fan W, Gao L, Sun J (2006) Tin oxide nanoparticle-functionalized multi-walled carbon nanotubes by the vapor phase method. *J Am Ceram Soc* 89(8):2671–2673
- [42] Jonge N, Allieux M, Doytcheva M, Kaiser M, Teo KBK, Lacerda RG et al (2004) Characterization of the field emission properties of individual thin carbon nanotubes. *Appl Phys Lett* 85(9):1607–1609
- [43] Doytcheva M, Kaiser M, Verheijen MA, Reyes-Reyes M, Terrones M, de Jonge N (2004) Electron emission from individual nitrogen-doped multi-walled carbon nanotubes. *Chem Phys Lett* 396(1–3):126–130
- [44] Brodie I, Spindt C (1992) Vacuum microelectronics. In: Hawkes PW (ed) *Advances in electronics and electron physics*. Elsevier, Amsterdam, pp 1–106
- [45] Gao R, Pan Z, Wang ZL (2001) Work function at the tips of multiwalled carbon nanotubes. *Appl Phys Lett* 78(12):1757–1759
- [46] Kurilich MR, Thapa A, Moilanen A, Miller JL, Li W, Neupane S (2019) Comparative study of electron field emission from randomly-oriented and vertically-aligned carbon nanotubes synthesized on stainless steel substrates. *J Vacuum Sci Technol B Nanotechnol Microelectron Mater Process Meas Phenom* 37(4):041202
- [47] Pandey A, Prasad A, Moscatello JP, Yap YK (2010) Stable electron field emission from PMMA–CNT matrices. *ACS Nano* 4(11):6760–6766
- [48] Chhowalla M, Ducati C, Rupesinghe NL, Teo KBK, Amaratunga GAJ (2001) Field emission from short and stubby vertically aligned carbon nanotubes. *Appl Phys Lett* 79(13):2079–2081
- [49] Patra R, Ghosh S, Sharma H, Vankar VD (2013) High stability field emission from zinc oxide coated multiwalled carbon nanotube film. *Adv Mater Lett* 4(11):849–855
- [50] Xu J, Xu P, Ou-Yang W, Chen X, Guo P, Li J et al (2015) Outstanding field emission properties of wet-processed titanium dioxide coated carbon nanotube based field emission devices. *Appl Phys Lett* 106(7):073501
- [51] Crespi VH, Chopra NG, Cohen ML, Zettl A, Louie SG (1996) Anisotropic electron-beam damage and the collapse of carbon nanotubes. *Phys Rev B* 54(8):5927–5931

- [52] Zhang K, Stocks GM, Zhong J (2007) Melting and premelting of carbon nanotubes. *Nanotechnology* 18(28):285703
- [53] Doytcheva M, Kaiser M, Jonge N (2006) In situ transmission electron microscopy investigation of the structural changes in carbon nanotubes during electron emission at high currents. *Nanotechnology* 17(13):3226–3233
- [54] Bocharov G, Eletsii A (2013) Theory of carbon nanotube (CNT)-based electron field emitters. *Nanomaterials* 3(3):393–442
- [55] Chen G, Neupane S, Li W, Chen L, Zhang J (2013) An increase in the field emission from vertically aligned multi-walled carbon nanotubes caused by NH₃ plasma treatment. *Carbon* 52:468–475

Publisher's Note Springer Nature remains neutral with regard to jurisdictional claims in published maps and institutional affiliations.